ACS OMEGA

http://pubs.acs.org/journal/acsodf

Mini-Review

Recent Progress and Challenges in $A_3Sb_2X_9$-Based Perovskite Solar Cells

Khursheed Ahmad and Shaikh M. Mobin*

Cite This: *ACS Omega* 2020, 5, 28404−28412

Read Online

ACCESS | Metrics & More | Article Recommendations | Supporting Information

ABSTRACT: The recent trends and current state of perovskite solar cells (PSCs) suggested their potential for practical applications. Since their origin, organic−inorganic lead halide ($MAPbX_3$) perovskite material-based PSCs have been widely attractive to the scientific community due to their simple manufacturing process, high performance, and cost effectiveness. In spite of the high performance, the lead halide perovskite solar cells are still agonizing due to the long-term stability and toxic nature of Pb. In the last 4 years or so, many alternative perovskite or perovskite-like materials were explored for the development of Pb-free PSCs. However, antimony (Sb)-based perovskite-like materials have shown enhanced stability and average photovoltaic performance. In this mini-review, we discuss the fabrication, recent trends, and current state of the Sb-based PSCs.

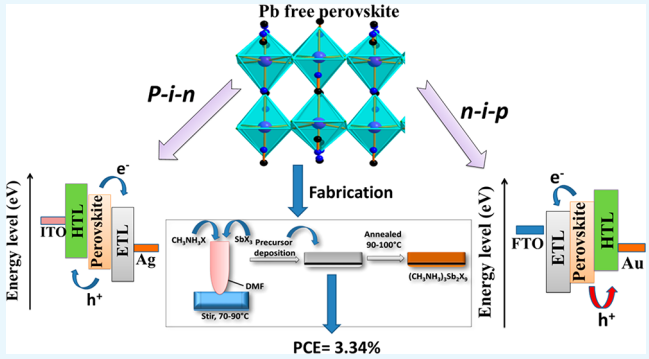

1. INTRODUCTION

The crystal structure of calcium titanate ($CaTiO_3$) was discovered in 1839 and named perovskite.[1] Perovskite is any material which satisfies the molecular formula of ABX_3 (A = Cs^+, $CH_3NH_3^+$, $NH_2CHNH_2^+$; B = Pb^{2+}, Sn^{2+}, Ge^{2+}; and X = halide anion) and has crystal structure similar to that of $CaTiO_3$. Several decades ago, a new perovskite structure $CsPbX_3$ was designed and synthesized by the reaction between lead halide and cesium iodide.[1] These perovskite structures have excellent optical and electrical properties which can be utilized in photovoltaic applications to produce the electrical energy on the consumption of sunlight.[2] The most important feature of these perovskite materials is their high absorption coefficient.[3] Although perovskite materials were prepared decades ago, they have been utilized as light absorbers in 2009 for photovoltaic applications.[3] Further, numerous strategies and approaches were used for the development of highly efficient perovskite solar cells (PSCs). Basically, Pb-based perovskite materials like $CsPbI_3$ and $CH_3NH_3PbI_3$ ($MAPbI_3$) have been widely explored in PSCs applications. Recently, the maximum power conversion efficiency (PCE) of >23% has been certified by NREL for Pb-based PSC.[4] It was believed that PSCs can be applied in practical applications, but their poor long-term stability and the toxic nature of Pb limits their potential for outdoor applications. Hence, a quest toward the development of Pb-free PSCs led researchers to venture for an alternate Pb-free perovskite material. Antimony (Sb) is a less toxic element which has the potential to replace the Pb from the perovskite structures for the construction of PSCs.[5] Jakubas et al.[6] investigated the structural properties of the $(CH_3NH_3)_3Sb_2I_9 = MA_3Sb_2I_9$ in 1991, whereas Bagautdinov et al.[7] studied the phase transition properties of the $Cs_3Sb_2I_9$ perovskite-like structure in 1999. Although these Sb-based perovskite-like materials were introduced in the early 1990's, their optoelectronic properties have been explored in the past few years. In this mini review, recent advances in the development of Sb-based PSCs have been summarized.

2. CONSTRUCTION OF PSCS

Different device architectures of PSCs have been reported so far which also plays a crucial role in controlling the performance of the PSCs. In general, PSCs consist of five different components, which are (i) conductive transparent glass substrate, (ii) electron transport layer, (iii) light absorber, (iv) hole transport layer, and (v) metal contact. The fabrications of some PSC device architectures associated with Sb are discussed in this section (see Supporting Information for details).

2.1. Synthesis of Thin Films of $A_3B_2X_9$ Perovskite-Like Materials. The quality of the prepared perovskite thin films influences the open circuit voltage and other photovoltaic parameters of the constructed PSCs. In this section, we

Received: August 28, 2020
Accepted: October 19, 2020
Published: November 2, 2020

https://dx.doi.org/10.1021/acsomega.0c04174
ACS Omega 2020, 5, 28404−28412

summarize various synthetic approaches utilized to develop the high-quality perovskite films for PSCs.

2.2. One-Step Method. A one-step approach is the most widely used method to prepare the perovskite thin films for PSCs applications. In this approach, methylammonium halide and metal halide have been dissolved in solvent (such as *N*,*N*-dimethylformamide (DMF) or dimethyl sulfoxide (DMSO) with overnight stirring at 70−90 °C to complete the reaction. Further, this precursor solution is spin-coated onto the patterned FTO substrate and annealed at 90−100 °C for 20−30 min (Scheme S1a).

2.3. Two-Step Deposition Method. The perovskite films prepared in one step suffer from poor surface morphological features and rapid crystallization. Thus, a two-step method was introduced to prepare the perovskite thin films with improved morphological features. In this method, step (i) SbX_3 in DMF is spin-coated onto the FTO glass substrate and annealed at 80−90 °C for 20−30 min. Further, antisolvents such as chlorobenzene or toluene are added to control the crystallization process, and in step (ii), CH_3NH_3X in 2-propanol is spin-coated and annealed at 80−90 °C for 20−30 min which resulted in the formation of high-quality thin films of $(CH_3NH_3)_3Sb_2X_9$ (Scheme S1b).

2.4. Sequential Deposition Method. This method has been used to improve the quality of the perovskite films. In this approach, SbX_3 in DMF is deposited onto the FTO glass substrate using the spin-coating method and annealed at 80−90 °C for 20−30 min. Further, this electrode is dipped in a solution of CH_3NH_3X in 2-propanol for 30−60 min and further annealed at 80−90 °C for 20−30 min. This yielded high-quality thin films of $(CH_3NH_3)_3Sb_2X_9$ (Scheme S1c).

3. STRUCTURAL AND OPTOELECTRONIC PROPERTIES OF $A_3B_2X_9$ PEROVSKITES

$A_3B_2X_9$ (A = Cs^+, Rb^+, K^+, $CH_3NH_3^+$, NH_4^+; B = Sb^{3+}; X = halide anion) perovskite-like materials possess excellent physiochemical and optoelectronic properties. $A_3B_2X_9$ perovskite-like materials were synthesized a few decades ago, but their structural and optoelectronic properties have been investigated recently. In the last 3−5 years, due to excellent aerobic stability $A_3B_2X_9$ perovskite-like materials have been employed as light absorbers for the construction of Pb-free PSCs.

3.1. Structural Properties of $A_3B_2X_9$ Perovskite-Like Materials. In 1992, Jakubas et al.[6] have synthesized and studied the phase transition properties of the $MA_3Sb_2I_9$, whereas $Cs_3Sb_2I_9$ was synthesized by Bagautdinov et al.[7] using the Bridgman method in 1999. Yang et al.[10] have found that the $MA_3Sb_2I_9$ possesses hexagonal $P6_3/mmc$ symmetry and crystal structure composed of antimony iodide octahedral layers with the voids between the layers filled with $CH_3NH_3^+$. Further, Yang et al.[10] also observed that in the case of replacing X = Br^- instead of I^-, $(CH_3NH_3)_3Sb_2Br_9$ shown trigonal $P\bar{3}m1$ symmetry. Zhang et al.[11] synthesized $(NH_4)_3Sb_2I_9$ crystals using a novel synthetic approach, $(NH_4)_3Sb_2I_9$ crystallizes in a monoclinic crystal system with $P2_1/n$ space group with a layered-type structure.[11] In 2017, Zuo et al.[12] also prepared $(NH_4)_3Sb_2I_9$ using antisolvent vapor-assisted crystallization. The crystal structure of $(NH_4)_3Sb_2I_9$, revealed central Sb atoms surrounded by six iodine atoms forming an octahedron, and nitrogen atoms were located at the tetrahedron center formed by four hydrogen atoms forming a 2D-layered structure. Furthermore, Buonassisi and co-workers have investigated the structural properties of all inorganic $Cs_3Sb_2I_9$, $Rb_3Sb_2I_9$, and $K_3Sb_2I_9$ perovskite-like materials.[13] The crystal structures of the $Cs_3Sb_2I_9$ (0D), $Rb_3Sb_2I_9$ (2D), and $K_3Sb_2I_9$ (2D) were obtained using Rietveld refinement (Figure 1A−C). The $Cs_3Sb_2I_9$ perovskite crystallizes in the

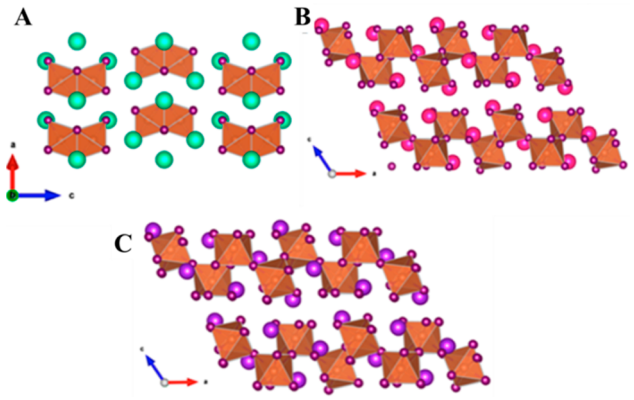

Figure 1. Crystal structures of $Cs_3Sb_2I_9$ (A), $Rb_3Sb_2I_9$ (B), and $K_3Sb_2I_9$ (C) perovskite-like materials. Reprinted with permission from ref 13. Copyright 2018 American Chemical Society.

$P6_3/mmc$ (no. 194) space group where $Sb_2I_9^{3-}$ dimers formed a 0D structure by sharing their triangular faces. In the case of $K_3Sb_2I_9$ and $Rb_3Sb_2I_9$, they crystallize in the $P\bar{3}m1$ space group with cations Rb or Cs or K acting as spacers between the corner-sharing octahedral layers and formed 2D-network structures with Rb or K cations.[13] This 2D structure formed when Rb or Cs or K acted as spacer between the corner-sharing octahedral layers and have space group of $P\bar{3}m1$.[13]

3.2. Optoelectronic Properties of $A_3B_2X_9$ Perovskites. The optical band gap of the light-absorbing materials is very crucial for the construction of high performance PSCs. Zuo et al.[12] have investigated the optical properties of the $(NH_4)_3Sb_2I_9$, which shows a band gap of 2.27 eV. In another work, Boopathi et al.[14] reported that $Cs_3Sb_2I_9$ has a band gap of 1.95 eV, whereas $MA_3Sb_2I_9$ (where MA = $CH_3NH_3^+$) has a band gap of 2.0 eV (Figure 2A,B). Buonassisi and co-workers investigated the optical properties of all inorganic $Cs_3Sb_2I_9$, $Rb_3Sb_2I_9$, and $K_3Sb_2I_9$ perovskite-like materials using UV−vis absorption spectroscopy.[13] The UV−vis spectra of the $Cs_3Sb_2I_9$, $Rb_3Sb_2I_9$, and $K_3Sb_2I_9$ perovskite-like materials revealed a band gap of 2.43, 2.03, and 2.02 eV, respectively (Figure 2C).

3.3. Progress in $A_3Sb_2X_9$ Perovskite-Based PSCs. *3.3.1. $(NH_4)_3Sb_2I_9$-Based PSC.* PSCs were developed in 2009 by Miyasaka and co-workers with PCE of 3%, and this PCE was boosted to 20% within a few years.[3,5] However, the poor stability of the Pb-based perovskite structure and the presence of Pb restricted their applications in large-scale production. Thus, numerous efforts have been made to develop highly stable PSCs with nontoxic or less toxic perovskite materials. Different metals such as Sn, Ge, Bi, Cu and Sb-based perovskite-like materials were employed for PSCs applications.[5] Zuo et al.[12] demonstrated the space charge limited current approach to determine the electron and hole mobility of the $(NH_4)_3Sb_2I_9$. Furthermore, Zuo et al.[12] tuned the optical properties of the $(NH_4)_3Sb_2I_9$ by making a series of thin films of the perovskite materials $(NH_4)_3Sb_2I_9$, $(NH_4)_3Sb_2I_6Br_3$, $(NH_4)_3Sb_2I_3Br_6$, and $(NH_4)_3Sb_2Br_9$ which showed optical band gaps of 2.27, 2.49, 2.66, and 2.78 eV,

https://dx.doi.org/10.1021/acsomega.0c04174
ACS Omega 2020, 5, 28404−28412

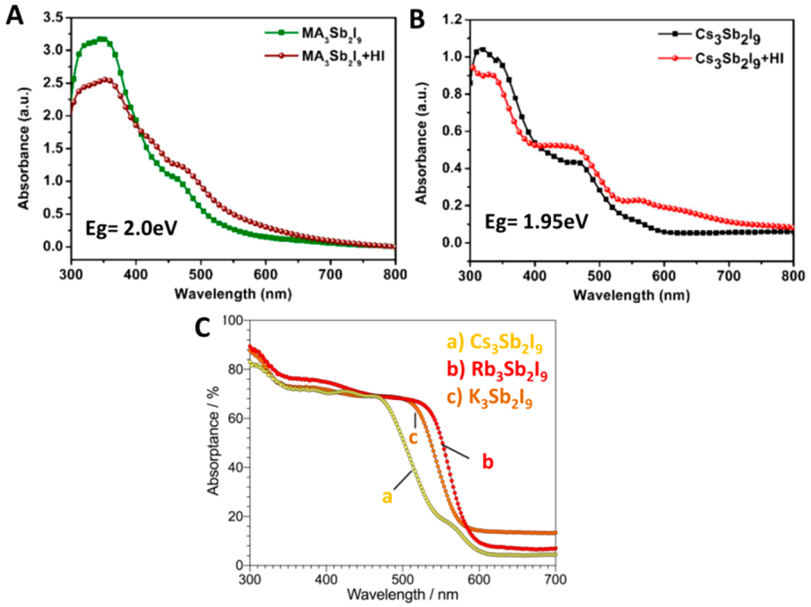

Figure 2. UV−vis spectra of $MA_3Sb_2I_9$ (A) and $Cs_3Sb_2I_9$ (B). Reprinted with permission from ref 13. Copyright 2018 American Chemical Society. UV−vis spectra of $Cs_3Sb_2I_9$, $Rb_3Sb_2I_9$, and $K_3Sb_2I_9$ perovskite materials (C). Reprinted with permission from ref 14. Copyright 2017 Royal Society of Chemistry.

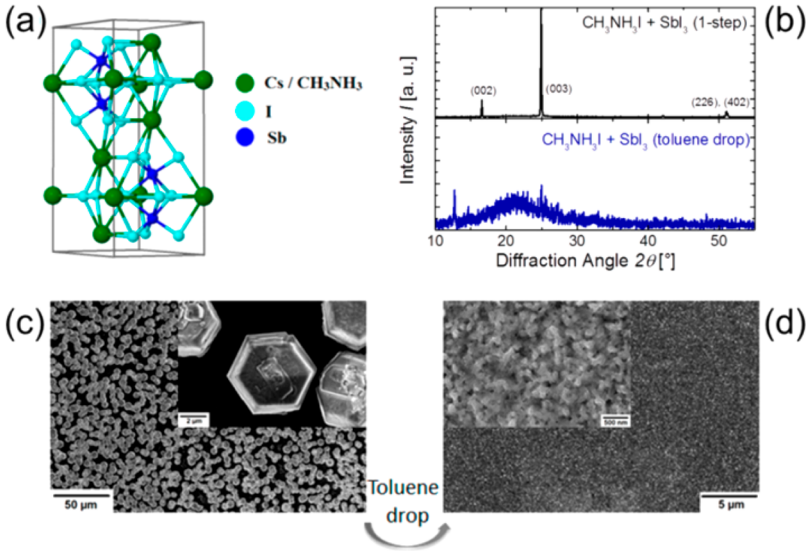

Figure 3. (a) Crystal structure of $MA_3Sb_2I_9$, (b) XRD patterns of the $MA_3Sb_2I_9$ thin films, (c) SEM images of the $MA_3Sb_2I_9$ thin films prepared by one-step, and (d) two-step method. Reprinted with permission from ref 8. Copyright 2016 American Chemical Society.

respectively. Further, planar PSC devices were fabricated, and the PSC devices developed exhibited PCE ranging between 0.01% and 0.51%. These obtained PCEs were poor, but the developed PSCs device exhibited excellent open circuit voltage of 1003 mV for $(NH_4)_3Sb_2I_9$ based device.

3.3.2. $MA_3Sb_2I_9$-Based PSCs. Hebig et al.[8] developed the PSCs using $MA_3Sb_2I_9$ as a visible light absorber. The $MA_3Sb_2I_9$ thin films were prepared under nitrogen atmosphere using a solvent engineering method by employing toluene as an antisolvent to control the crystallization process. The $MA_3Sb_2I_9$ crystallizes in the $P6_3/mmc$ space group and the crystal structure is similar to that of $MA_3Bi_2I_9$ and $Cs_3Sb_2I_9$ (Figure 3a).[8] The crystal structure of $MA_3Sb_2I_9$ shows that $(Sb_2I_9)^{3-}$ is surrounded by three $(CH_3NH_3)^+$ cations by hydrogen bonding interactions. The XRD patterns of the $MA_3Sb_2I_9$ thin films prepared by one-step and two-step methods are shown in Figure 3b. The $MA_3Sb_2I_9$ thin films prepared by one step showed a crystalline nature, whereas amorphous characters were present in the $MA_3Sb_2I_9$ thin films prepared by a two-step method (Figure 3b). This amorphous nature may be due to toluene. The hexagonal surface morphology (Figure 3c) was observed for $MA_3Sb_2I_9$ thin films prepared by a one-step method, whereas a nonhexagonal homogeneous and pinhole-free surface was obtained for $MA_3Sb_2I_9$ thin films prepared by a two-step method (Figure 3d) by employing SEM.

The optoelectronic properties of $MA_3Sb_2I_9$ thin films were investigated, which showed higher absorption coefficient of $\alpha > 10^5$ cm^{-1} with a band gap of 2.14 eV which makes it a potential candidate for tandem solar cell applications.

https://dx.doi.org/10.1021/acsomega.0c04174
ACS Omega 2020, 5, 28404−28412

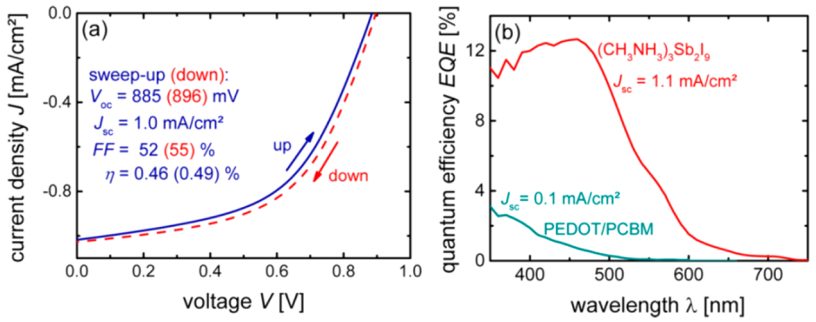

Figure 4. *J*−*V* curves (a) and EQE (b) of the PSCs (ITO/PEDOT:PSS (25 nm)/absorber/PC61BM (60 nm)/ZnO-NP (60 nm)/Al (150 nm). Reference device: ITO (120 nm)/PEDOT/PCBM/ZnO-NP/Al (green). Reprinted with permission from ref 8. Copyright 2016 American Chemical Society.

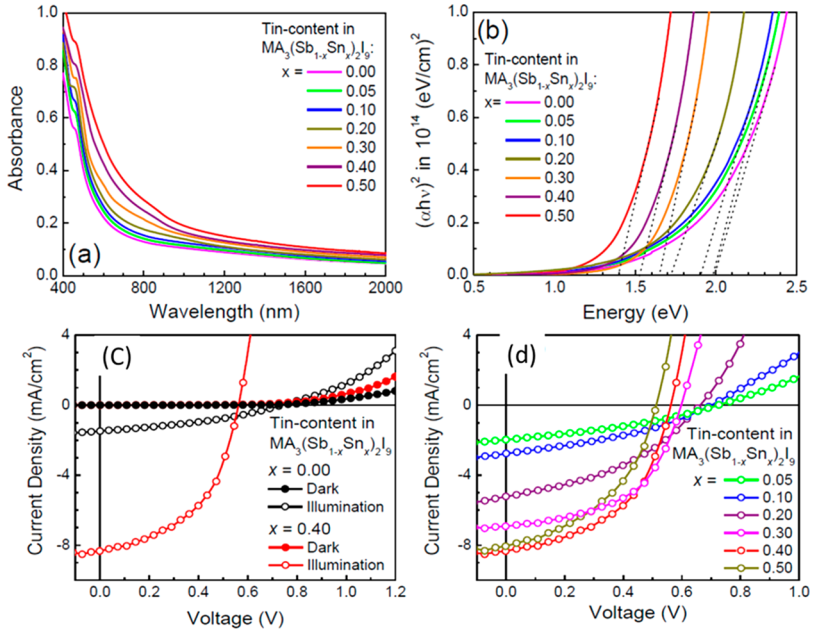

Figure 5. UV−vis spectra (a) and Tauc plot (b) of the $MA_3Sb_2I_9$ doped with different Sn content. *J*−*V* curves of the PSCs based on $MA_3(Sb_{1-x}Sn_x)_2I$ with x = 0 and 0.40 (c) and x = 0.05, 0.10, 0.20, 0.30, 0.40, and 0.50 (d). Reprinted with permission from ref 16. Copyright 2018 American Chemical Society.

The planar PSCs were developed using $MA_3Sb_2I_9$ light absorber, and photovoltaic performance was determined by short circuit photocurrent density−voltage (*J*−*V*) curves. The *J*−*V* curves of the fabricated PSCs (ITO/PEDOT:PSS(25 nm)/absorber/PC61BM(60 nm)/ZnO-NP(60 nm)/Al(150 nm) exhibited PCE of 0.49% with good open circuit voltage of 896 mV (Figure 4a). The external quantum efficiency (EQE) of the fabricated PSCs with device architectures (ITO/PEDOT:PSS (25 nm)/absorber/PC61BM(60 nm)/ZnO-NP (60 nm)/Al (150 nm) and ITO(120 nm)/PEDOT/PCBM/ZnO-NP/Al) were also investigated (Figure 4b). Boopathi et al.[14] have obtained the high-quality thin films of $MA_3Sb_2I_9$ by using additive such as hydroiodic acid (HI) to control the formation of $MA_3Sb_2I_9$ thin films. The constructed PSCs with and without HI additive showed PCE of 2.04% and 1.11%, respectively. In another recent report, Giesbrecht et al.[15] also reported the preparation of 2D layered $MA_3Sb_2I_9$ for solar cell applications. The $MA_3Sb_2I_9$ 2D films were grown using antimony acetate precursor under glovebox. They have shown that 2D layered $MA_3Sb_2I_9$ is a more efficient light absorber compared to the 0D $MA_3Sb_2I_9$. The optoelectronic properties of the 0D and 2D layered $MA_3Sb_2I_9$ were investigated. The direct and indirect band gap of the 2D layered $MA_3Sb_2I_9$ was found to be 2.13 and 2.01 eV, respectively. In the case of 0D $MA_3Sb_2I_9$, the absorption band was observed between 450 and 500 nm which suggested that 0D $MA_3Sb_2I_9$ has a wide band gap. The PSCs was fabricated using SnO_2 and TiO_2 as compact and mesoporous layer, respectively. The highest PCE of 0.54% was achieved using TiO_2 layer, whereas the lower PCE of 0.36% was reported for c-SnO_2 based PSCs. The open circuit voltage of 570 mV was also reported for c-SnO_2 based PSCs, which may be due to the better charge transport or lower recombination reactions. In 2020, Shaikh and co-workers have developed the PSCs using $MA_3Sb_2I_9$ as light absorber[5] by employing a two-step sequential deposition method to prepare the high-quality thin films of $MA_3Sb_2I_9$. The sequential deposition method led to the formation of a uniform film of $MA_3Sb_2I_9$ with a band gap of 2.1 eV. The highest occupied molecular orbital (HOMO) and lowest unoccupied molecular orbital (LUMO) energy level values of the $MA_3Sb_2I_9$ were also determined by the combined study of cyclic voltammetry and UV−vis absorption spectroscopy. The constructed PSCs device with a two-step sequential deposition method showed

https://dx.doi.org/10.1021/acsomega.0c04174
ACS Omega 2020, 5, 28404−28412

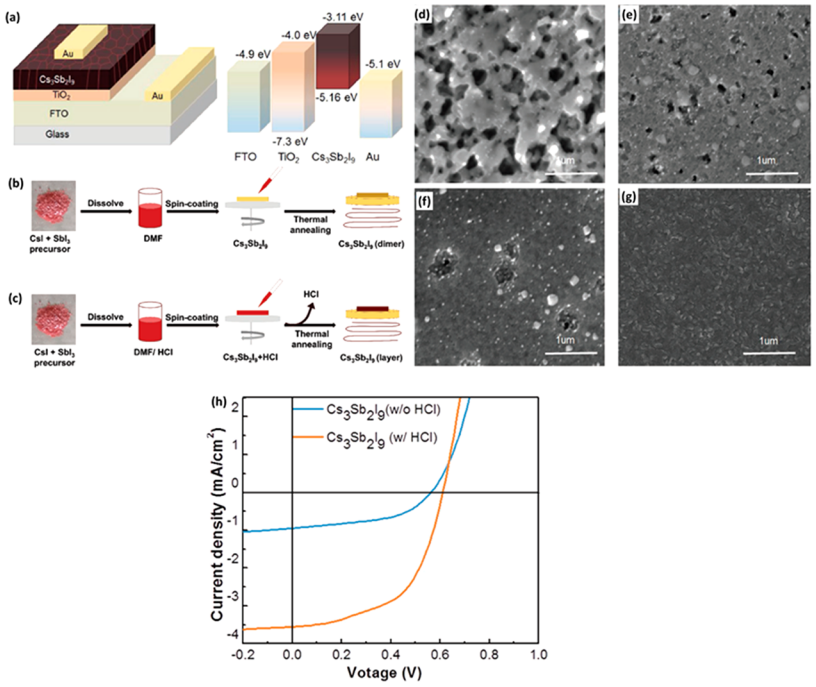

Figure 6. Schematic diagram of PSCs device and energy level diagram (a). Schematic synthetic view of $Cs_3Sb_2I_9$ without (b) and with (c) HCl. SEM images of the $Cs_3Sb_2I_9$ thin films prepared without antisolvent (d) and with antisolvents of toluene (e), chlorobenzene (f), and isopropanol (g). *J*−*V* curves of the PSCs device (h). Reprinted with permission from ref 18. Copyright 2019 John Wiley and Sons.

the higher PCE of 0.54% with good open circuit voltage of 740 mV compared to the one-step approach (PCE = 0.1% and V_{oc} = 690 mV). Authors have concluded that this improved PCE was attributed to the high-quality thin films (larger grain size, nonhexagonal surface morphology, and uniform surface coverage) and better charge extraction/electron transportation. It is believed that the morphological features of the absorber layer influence the photovoltaic parameters and performance of the PSCs.

It is noteworthy to understand that the band gap of the absorber layer plays a crucial role and $MA_3Sb_2I_9$ falls in the band gap range of 1.95−2.2 eV. The band gap of the perovskite materials can be easily tuned by doping with transition metals.[16] Thus, Pal and co-workers inserted the Sn(IV) to the $MA_3Sb_2I_9$ to obtain the low band gap light absorbers for photovoltaic applications.[16] Here, authors have successfully employed Sn(IV) as a dopant due to its stability and less toxic nature. Different Sn(IV) contents (0%, 0.05%, 0.10%, 0.20%, 0.30%, 0.40%, and 0.50%) were explored to dope the $MA_3Sb_2I_9$. The UV−vis spectra of the Sn(IV) doped $MA_3(Sb_{1-x}Sn_x)_2I$ (x = 0%, 0.05%, 0.10%, 0.20%, 0.30%, 0.40%, and 0.50%) were investigated to understand the impact of doping on the optical properties of $MA_3Sb_2I_9$ (Figure 5a). The lowest band gap of 1.40 eV was found for $MA_3(Sb_{1-x}Sn_x)_2I$ with x = 0.50, whereas the higher band gap of 2.0 eV was reported for $MA_3(Sb_{1-x}Sn_x)_2I$ with x = 0 (Figure 5b). This showed that the increase of the Sn(IV) content reduced the band gap. Further, authors developed the *p-i-n* heterojunction PSCs with Cu@NiO and ZnO as hole and electron transporting layers, respectively. The highest PCE of 2.69% was achieved for the PSCs device developed using $MA_3(Sb_{1-x}Sn_x)_2I$ with x = 0.40 (Figure 5c). On the other hand, the lowest PCE of 0.57% was reported for $MA_3(Sb_{1-x}Sn_x)_2I$ with x = 0 based PSCs (Figure 5d). This suggested that the $MA_3Sb_2I_9$ with narrow band gap and good morphological features may be a suitable candidate for photovoltaic applications.

Nazeeruddin and co-workers also proposed a benign approach to control the dimensional growth and facilitate the heterogeneous nucleation by employing bis-(trifluoromethane)sulfonimide lithium (LiTFSI). The introduction of LiTFSI led to the formation of 2D $MA_3Sb_2I_{9-x}Cl_x$ films which showed the band gap of 2.05 eV. The highest PCE of 3.34% was reported with LiTFSI, while the lower PCE of 1.37% was achieved in the absence of LiTFSI.[10] Authors also reported the excellent stability of the PSCs over 1400 h in ambient conditions.

3.3.3. $Cs_3Sb_2I_9$-Based PSCs. All inorganic perovskite structures possess relatively higher stability compared to the organic−inorganic hybrid perovskite structures. Mitzi and co-workers reported the properties of the $Cs_3Sb_2I_9$ and explored its potential for photovoltaic applications.[17] The band gap of the $Cs_3Sb_2I_9$ was found to be 2.05 eV. The PSCs with glass/FTO/c-TiO_2/$Cs_3Sb_2I_9$/PTAA/Au architecture exhibited open circuit voltage of 307 mV.[17] Chu and co-workers also employed the $Cs_3Sb_2I_9$ as a light absorber layer for Pb-free PSCs applications.[14] They have constructed the PSCs with planar architecture and reported a PCE of 0.67%. Further, to improvise the morphological features, controlled surface, and to obtain uniform thin films, HI treatment was given to the $Cs_3Sb_2I_9$ perovskite which led to enhanced PCE of 0.84%.

In general, the $Cs_3Sb_2I_9$ exists in two different polymorphs, viz., 0D (dimer) and 2D (layered), where the dimer phase has a band gap of 2.50 eV, whereas layered $Cs_3Sb_2I_9$ perovskite exhibits a band gap of 2.05 eV. The layered $Cs_3Sb_2I_9$ also has an excellent absorption coefficient which makes it suitable for photovoltaic applications. Umar et al.[18] developed the PSCs with mesoscopic structure using $Cs_3Sb_2I_9$ light absorber layer. The dimer phase of $Cs_3Sb_2I_9$ was obtained in the absence of HCl, whereas the layered structure of $Cs_3Sb_2I_9$ was obtained in

https://dx.doi.org/10.1021/acsomega.0c04174
ACS Omega 2020, 5, 28404−28412

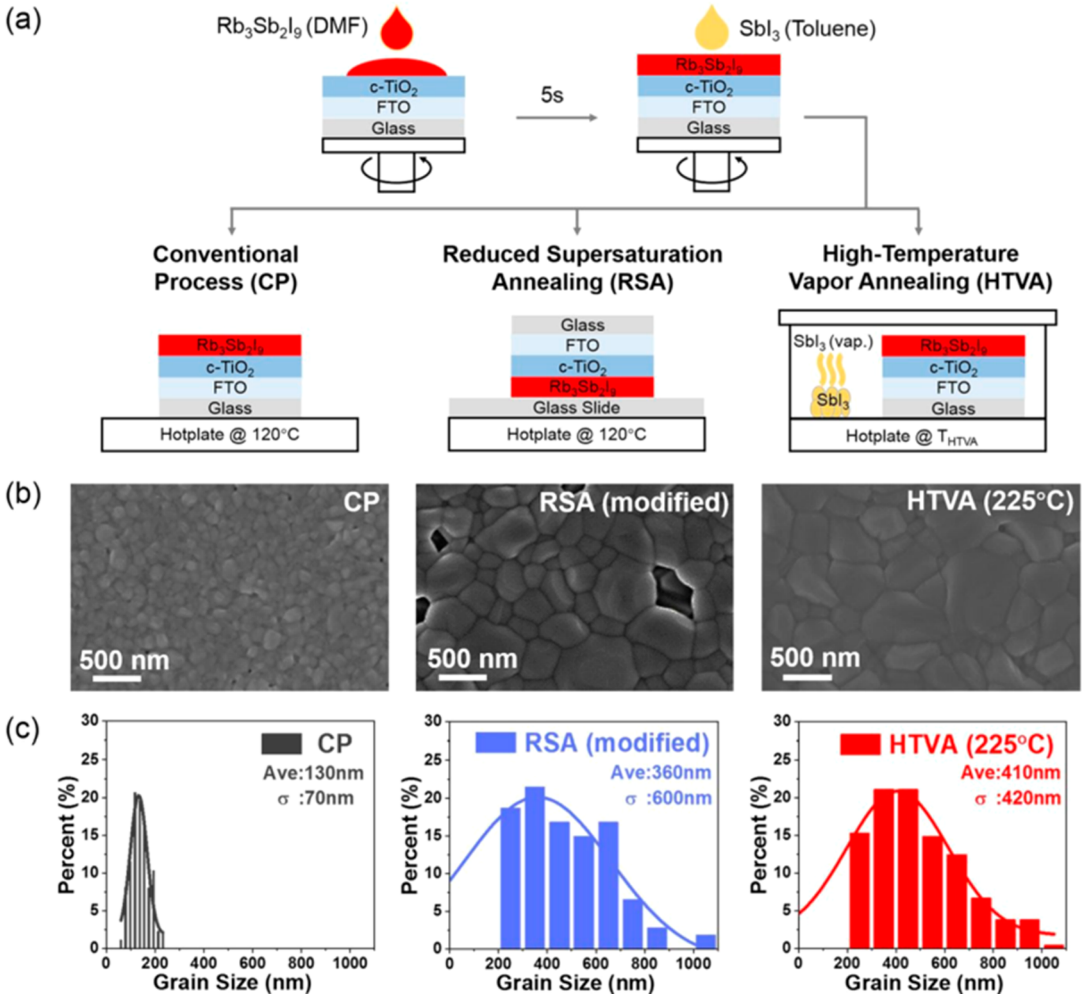

Figure 7. (a) Depiction of essential process step in CP, RSA, and HTVA. (b) SEM images of the resulting films and (c) corresponding grain size distributions. Reprinted with permission from ref 24a. Copyright 2020 Royal Society of Chemistry.

the presence of HCl. The $Cs_3Sb_2I_9$ thin films were also prepared in the absence and presence of antisolvents (toluene, chlorobenzene, and isopropanol). The device structure and energy level diagram of the PSCs is shown in Figure 6a, and the synthesis route is shown in Figure 6b,c. According to the SEM results (Figure 6d−g), the grain size and improved crystallization was observed in the case of toluene (Figure 6e) and chlorobenzene (Figure 6f), but some voids were still present. The highly uniform and pinhole/void-free $Cs_3Sb_2I_9$ thin films were obtained in the presence of isopropanol (Figure 6g). However, in the absence of antisolvents, poor crystallization of the $Cs_3Sb_2I_9$ thin film was observed (Figure 6d). This suggested that the presence of isopropanol as antisolvent could avoid the short circuit and reduce the trap states. The improved PCE of 1.21% was achieved with HCl, whereas the lower PCE of 0.43% was observed in the absence of HCl additive (Figure 6h). Singh et al.[19] also found better photovoltaic properties in the $Cs_3Sb_2I_3$ material with layered polymorph phase (band gap of 2.05 eV) compared to the dimer polymorph (band gap of 2.3 eV) of $Cs_3Sb_2I_3$. The constructed PSCs with inverted planar heterojunction architecture (ITO/PEDOT:PSS/$Cs_3Sb_2I_9$/$PC_{70}BM$/C_{60}/BCP/Al) exhibited the best PCE of 1.5% using $Cs_3Sb_2I_3$ perovskite with layered phase. However, relatively lower PCE of 0.83% was achieved for $Cs_3Sb_2I_3$ with the dimer form. This may be due to the relatively lower band gap and better optoelectronic properties of the layered $Cs_3Sb_2I_3$ structure. Further, to address the most important aspect of the device, the stability of these all-inorganic perovskite materials was also explored. The stability of the $Cs_3Sb_2I_3$ polymorphs (dimer and layered) was studied by Chonamada et al.,[20] and they found that the dimer form of the $Cs_3Sb_2I_3$ degraded in 49 days whereas the layered form degraded in 88 days. Authors also found that water, heat, and light equally cause the degradation of $Cs_3Sb_2I_3$. This showed that $Cs_3Sb_2I_3$ can be employed as an efficient light absorber layer for Pb-free PSCs applications.

3.3.4. $Rb_3Sb_2I_9$-Based PSCs. Johnston et al.[21a] investigated the properties of $Rb_3Sb_2I_9$ nanoparticles as a newer class of perovskite material which has a direct and indirect band gap of 2.24 and 2.1 eV, respectively. Harikesh et al.[22a] reported photovoltaic properties of the $Rb_3Sb_2I_9$ and found that $Rb_3Sb_2I_9$ has *P*1*c*1 space group. Authors also found that $Rb_3Sb_2I_9$ is thermally stable up to 250 °C. The PSCs device with mesoscopic structure exhibited the PCE of 0.66% with open circuit voltage of 550 mV. According to the theoretical investigations, it was proposed that $Rb_3Sb_2I_9$ with layered structure can achieve the highest photocurrent density of ∼10 mA/cm^2. The $Rb_3Sb_2I_9$ has good stability and absorption coefficient, which makes it another suitable Pb-free light absorber material. Since the cationic group influences the

https://dx.doi.org/10.1021/acsomega.0c04174
ACS Omega 2020, 5, 28404−28412

Table 1. Photovoltaic Parameters of the Reported PSCs with Different Light Absorbers

sample	absorber layer	FF (%)	V_{oc} (V)	J_{sc} (mA/cm^2)	PCE (%)	ref
1.	$MA_3Sb_2I_{9-x}Cl_x$	65	0.70	7.38	3.34	10
2.	$(NH_4)_3Sb_2I_9$	42.5	1.03	1.15	0.51	12
3.	$Rb_3Sb_2I_9$	63	0.66	1.84	0.76	13
4.	$K_3Sb_2I_9$	50	0.338	0.41	0.07	13
5.	$Cs_3Sb_2I_9$	58	0.404	0.13	0.03	13
6.	$MA_3Sb_2I_9$+HI	60	0.62	5.41	2.04	14
7.	$Cs_3Sb_2I_9$+HI	48	0.60	2.91	0.84	14
8.	$MA_3Sb_2I_9$	52	0.46	2.21	0.54	15
9.	$MA_3Sb_2I_9$	47	0.74	1.40	0.54	5
10.	Sn doped $MA_3Sb_2I_9$	58	0.56	8.32	2.70	16
11.	$Cs_3Sb_2I_9$	37	0.68	4.62	1.26	19
12.	$Rb_3Sb_2I_9$	57	0.55	2.11	0.66	22
13.	$Rb_3Sb_2I_9$	40	0.61	5.54	1.35	24
14.	Bromoantimonate (V) (N-EtPy)[$SbBr_6$]	58	1.2	5.1	2.50	9
16.	$MASbSI_2$	58	0.65	8.12	3.08	25a

exciton binding energy, structural dimensionality, optoelectronic and photovoltaic performance, Buonassisi and co-workers investigated the optical/photovoltaic properties of the various perovskite-like materials ($K_3Sb_2I_9$, $Cs_3Sb_2I_9$, and $Rb_3Sb_2I_9$).[13] The $K_3Sb_2I_9$, $Cs_3Sb_2I_9$, and $Rb_3Sb_2I_9$ have band gap of 2.02, 2.43, and 2.03 eV, respectively, and revealed that $K_3Sb_2I_9$ and $Cs_3Sb_2I_9$ exhibited poor PCE whereas $Rb_3Sb_2I_9$-based PSCs showed improved PCE of 0.76%. Weber et al.[23a] studied the effect of iodide to bromide ratio and tuned the band gap of the $Rb_3Sb_2I_9$. The optical band gap was changed by tuning the halide composition ($Rb_3Sb_2I_9$, $Rb_3Sb_2Br_{9-x}I_x$, and $Rb_3Sb_2Br_9$) and the fabricated PSCs (*n-i-p* solar cell structure) showed the best PCE of 1.37% with excellent photocurrent density (4.25 mA/cm^2) and exhibited the excellent stability up to 150 days for $Rb_3Sb_2I_9$-based PSCs, and 85% of the initial PCE was retained. The perovskite light absorber with large grain size improves the carrier mobility, influencing the performance of the PSCs and lifetime. Thus, photovoltaic performance of the PSCs can be enhanced by extending the carrier drift/diffusion length. So far, the largest grain size of the $Rb_3Sb_2I_9$ was found to be 200 nm. Therefore, it will be of great significance to prepare the $Rb_3Sb_2I_9$ thin films with larger grain size for efficient photovoltaic devices. In this regard, Li et al.[24a] obtained the conventional process (CP), high-temperature vapor annealing (HTVA), and reduced supersaturation annealing (RSA) processed $Rb_3Sb_2I_9$ perovskite thin films (Figure 7a). The HTVA processed $Rb_3Sb_2I_9$ thin film showed the smooth film surface (Figure 7b), larger grains (600 nm), and void-free surface compared to the RSA-processed $Rb_3Sb_2I_9$ thin film (Figure 7c).

Accordingly, the best PCE of 1.35% was obtained for HTVA processed $Rb_3Sb_2I_9$ thin film based PSCs, whereas the relatively lower PCE of 1.12% was achieved for RSA processed $Rb_3Sb_2I_9$ thin film. The poor PCE of 0.38% was reported for the CP processed $Rb_3Sb_2I_9$ thin film. The PCE of the HTVA processed $Rb_3Sb_2I_9$ thin film based PSCs was due to the larger grain size, which improved the carrier mobility and lifetime.

3.3.5. Other Sb-Based Perovskite Like Materials. Adonin et al.[9] investigated the optical and photovoltaic features of the *N*-ethylpyridinium bromoantimonate (V) = (N-EtPy)[$SbBr_6$] and developed the inverted planar PSCs. The (N-EtPy)-[$SbBr_6$] materials has a band gap of 2.25 eV, which suggested its potential as energy material for tandem solar cells. Authors developed the inverted planar PSCs with different electron transport layers (6,6-phenyl C61 butyric acid methyl ester = PCBM and *N,N′*-bis(2-ethylhexyl)-perylenediimide = PDI). The PSCs with PCBM achieved the PCE of 2.8%, whereas the device fabricated with PDI as electron transport layer showed PCE of 3.2%.[9] The photovoltaic performance of the inverted planar PSCs (ITO/PEDOT:PSS/1/PDI/Ag) were also compared with standard device architecture (ITO/TiOx/1/P_3HT/Au). The standard device architecture of PSCs exhibited the improved PCE of 3.8%, which may be due to the better charge extraction and fast electron transport process. Moreover, the higher open circuit voltage of 1285 mV was achieved using standard device architecture.[9] This work suggested that the photovoltaic performance of the PSCs may be further improved by reducing recombination reactions and improving charge extraction. Li et al.[21b] reported 0D tetranuclear perovskite-like material heteromorphic hybrids [$(C_7H_{18}N_2O)_3Sb_4I_{18}\cdot H_2O$ and $(C_7H_{18}N_2O)Sb_2I_8\cdot H_2O$ (where $C_7H_{18}N_2O^{2+}$ = *N*-aminopropylmorpholinium)]. The $(C_7H_{18}N_2O)_3Sb_4I_{18}\cdot H_2O$ and $(C_7H_{18}N_2O)Sb_2I_8\cdot H_2O$ exhibited the optical band gap of 1.71 and 2.11 eV, respectively. This kind of perovskite-like hybrid material has the potential for use in photovoltaic applications. Jia et al.[22b] reported Cu_3SbI_6 as a light absorber, which has indirect band gap of 2.43 eV. They constructed the PSCs with device structure of ITO/PEDOT:PSS/Cu_3SbI_6/$PC_{61}BM$/Al, which showed the good open circuit voltage of 704 mV along with the PCE of 0.50%. Deng and co-workers proposed a new antimony−silver halide double perovskite light absorber ($(CH_3NH_3)_2AgSbI_6$) for photovoltaic applications.[23b] This perovskite, $(CH_3NH_3)_2AgSbI_6$, has a band gap of 1.93 eV and showed good stability up to 370 days. Vargas et al.[24b] also reported a direct band gap of copper−antimony halide perovskite material ($Cs_4CuSb_2Cl_{12}$) and investigated its optoelectronic properties. The $Cs_4CuSb_2Cl_{12}$ perovskite showed good stability and has a very narrow band gap of 1.02 eV, which suggested its potential application in the development of Pb free PSC. Nie et al.[25b] reported methylammonium antimony sulfur diiodide (MASb-SI_2) perovskite-like structure (band gap = 2.03 eV) as light absorber, and the PSCs device exhibited good PCE of 3.08%. The photovoltaic performance of the Sb-based PSCs have been summarized in Table 1.

https://dx.doi.org/10.1021/acsomega.0c04174
ACS Omega 2020, 5, 28404−28412

4. CONCLUSIONS AND FUTURE PERSPECTIVES

Antimony (Sb)-based perovskite materials are an emerging class of perovskite-like materials with good optoelectronic features. In the past few years, compared to the Pb-based perovskite materials, Sb-based perovskite-like materials have excellent stability and less toxic nature, which makes them alternative potential light absorbers for Pb-free PSCs applications. The band gap of the Sb-based perovskite-like materials lies in the range of 1.95−2.43 eV, attempts are made to reduce the band gap by insertion of less toxic metal to the Sb-based perovskite-like structures. So far, to the best of our knowledge, the best developed perovskite solar cells devices based on Sb-based perovskite-like structures exhibited the highest PCE of 3.34%, which is remarkably good performance compared to the other nontoxic perovskite materials. The research on Sb-based perovskite-like materials is still in the initial phase in terms of PCE and still needs to be further improved by employing novel approaches. The major challenges with Sb-based perovskite-like materials are wide band gap, poor morphological features, uncontrolled crystallization process, poor electron transportation, and water sensitivity. These challenges may be addressed by the following efforts: (i) the wide band gap should be narrowed by inserting less toxic and highly stable metals, (ii) the morphological features and crystallization process can be controlled by introducing new additives and antisolvents, (iii) the design and synthesis of new charge extraction layers/electron transport layers would be of great significance to improve the performance of the perovskite solar cells, and (iv) the water sensitivity of the Sb-based perovskite-like materials can be improved by introducing hydrophobic cations to the perovskite structures.

■ ASSOCIATED CONTENT

Supporting Information

The Supporting Information is available free of charge at https://pubs.acs.org/doi/10.1021/acsomega.0c04174.

Construction of PSCs (PDF)

■ AUTHOR INFORMATION

Corresponding Author

Shaikh M. Mobin − *Discipline of Chemistry, Discipline of Biosciences and Biomedical Engineering (BSBE), and Discipline of Metallurgy Engineering and Material Science (MEMS), Indian Institute of Technology Indore, Indore 453552, Madhya Pradesh, India;* orcid.org/0000-0003-1940-3822; Phone: +91-7312438752; Email: xray@iiti.ac.in

Author

Khursheed Ahmad − *Discipline of Chemistry, Indian Institute of Technology Indore, Indore 453552, Madhya Pradesh, India*

Complete contact information is available at: https://pubs.acs.org/10.1021/acsomega.0c04174

Notes

The authors declare no competing financial interest.

Biographies

Dr. Khursheed Ahmad has completed Ph.D. in the Discipline of Chemistry, Indian Institute of Technology Indore, India. After Ph.D., Dr. Khursheed Ahmad continued his research work with Dr. Shaikh M Mobin, Discipline of Chemistry IIT Indore. His current research interests include perovskite solar cells, especially lead-free perovskite solar cells, electrochemical sensors, and wastewater treatment (photocatalysis and adsorption).

Dr. Shaikh M. Mobin accomplished his Bachelor's and Master's degrees from Wilson College, University of Mumbai with major in Chemistry and Ph.D. from Mumbai University in Chemistry. In 2012, he joined IIT Indore and is now working as an Associate Professor in the Discipline of Chemistry. He had developed his multidisciplinary research group working in a wide area of research including solid-state structural transformation, design and synthesis of newer class of MOFs and their applications in energy storage, conversion and biomedical devices, exploring metal nano-oxide materials for energy storage, conversion, optical and electrochemical sensing, metal nano-oxide materials derived by employing metal complexes/MOFs as single-source molecular precursors as catalyst in organic transformation, and developing greener c-dots for bioimaging and biomarkers. Moreover, the research group designs and synthesizes small molecules as cellular organelles target and docking. Finally, our group at IIT Indore is also involved in the development of advanced and novel materials for all aspects of solar energy harvesting and perovskite-based lead-free solar cells including absorber material, electrode materials, hole-transport, and electron acceptor materials as well as blocking layer.

■ ACKNOWLEDGMENTS

K.A. would like to thank UGC, New Delhi, India (Scheme No./RGNFD/2014-15) for research fellowship. S.M.M. would like to thank CSIR, New Delhi, India for financial support (File no. 01(2935)/18/EMR-II). Authors sincerely acknowledged Discipline of Chemistry, IIT Indore for research grant.

■ REFERENCES

(1) Kour, R.; Arya, S.; Verma, S.; Gupta, J.; Bandhoria, P.; Bharti, V.; Datt, R.; Gupta, V. Potential Substitutes for Replacement of Lead in Perovskite Solar Cells: A Review. *Global Challenges* **2019**, *3*, 1900050.

(2) (a) Ahmad, K.; Mobin, S. M. Graphene Oxide based Planar Heterojunction Perovskite Solar Cell under Ambient Condition. *New J. Chem.* **2017**, *41*, 14253−14258. (b) Jiang, F.; Yang, D.; Jiang, Y.; Liu, T.; Zhao, X.; Ming, O. Y.; Luo, B.; Qin.; et al. Chlorine-Incorporation-Induced Formation of the Layered Phase for Antimony-Based Lead-Free Perovskite Solar Cells. *J. Am. Chem. Soc.* **2018**, *140*, 1019−1027.

(3) Kojima, A.; Teshima, K.; Shirai, Y.; Miyasaka, T. Organometal halide perovskites as visible-light sensitizers for photovoltaic cells. *J. Am. Chem. Soc.* **2009**, *131*, 6050−6051.

(4) Kanda, H.; Shibayam, N.; Huckab, A. J.; Lee, Y.; Paek, S.; Klipfel, N.; Roldan-Carmona, C.; Queloz, V. E.; Grancini, G.; Zhang.; et al. Band-bending Induced Passivation: High Performance and Stable Perovskite Solar Cells using a Perhydropoly(silazane) Precursor. *Energy Environ. Sci.* **2020**, *13*, 1222−1230.

(5) Ahmad, K.; Kumar, P.; Mobin, S. M. A Two-Step Modified Sequential Deposition Method-based Pb-Free $(CH_3NH_3)_3Sb_2I_9$ Perovskite with Improved Open Circuit Voltage and Performance. *ChemElectroChem* **2020**, *7*, 946−950.

(6) Jakubas, R.; Decressain, R.; Lefebvre, J. NMR and Dilatometric Studies of the Structure Phase transitions of $(CH_3NH_3)_3Sb_2I_9$, and $(CH_3NH_3)_3Bi_2I_9$ Crystal. *J. Phys. Chem. Solids* **1992**, *53*, 755−759.

(7) Bagautdinov, B.; Novikova, M. S.; Aleksandrova, I. P.; Blomberg, M. K.; Chapuis, G. X-ray study of phase transitions in $Cs_3Sb_2I_9$ crystal. *Solid State Commun.* **1999**, *111*, 361−366.

(8) Hebig, J. C.; Kühn, I.; Flohre, J.; Kirchartz, T. Optoelectronic Properties of $(CH_3NH_3)_3Sb_2I_9$Thin Films for Photovoltaic Applications. *ACS Energy Lett.* **2016**, *1*, 309−314.

(9) Adonin, S. A.; Frolova, L. A.; Sokolov, M. N.; Shilov, G. V.; Korchagin.; et al. Antimony (V) Complex Halides: Lead-Free

Perovskite-Like Materials for Hybrid Solar Cells. *Adv. Energy Mater.* **2018**, *8*, 1701140.
(10) Yang, Y.; Liu, C.; Cai, M.; Liao, Y.; Ding, Y.; Ma, S.; Liu, X.; Guli, M.; Dai, S.; Nazeeruddin, M. K. Dimension-controlled Growth of Antimony-based Perovskite-like Halide for Lead-free and Semi-transparent Photovoltaics. *ACS Appl. Mater. Interfaces* **2020**, *12*, 17062−17069.
(11) Zhang, H.; Fang, L.; Yuan, R.-Z. Triammonium nonaiododiantimonate(III), $(NH_4)_3[Sb_2I_9]$. *Acta Crystallogr., Sect. E: Struct. Rep. Online* **2005**, *61*, i70−i72.
(12) Zuo, C.; Ding, L. Lead-free Perovskite Materials $(NH_4)_3Sb_2I_xBr_{9-x}$. *Angew. Chem., Int. Ed.* **2017**, *56*, 6528−6532.
(13) Correa-Baena, J. P.; Nienhaus, L.; Kurchin, R. C.; Shin, S. S.; Wieghold, S.; Hartono.; et al. A-Site Cation in Inorganic $A_3Sb_2I_9$ Perovskite Influences Structural Dimensionality, Exciton Binding Energy, and Solar Cell Performance. *Chem. Mater.* **2018**, *30*, 3734−3742.
(14) Boopathi, K. M.; Karuppuswamy, P.; Singh, A.; Hanmandlu, C.; Lin, L.; Abbas, S. A.; Chang, C. C.; Wang, P. C.; Li, G.; Chu, C. W. Solution-Processable Antimony-based Light-absorbing Materials Beyond Lead Halide Perovskites. *J. Mater. Chem. A* **2017**, *5*, 20843−20850.
(15) Giesbrecht, N.; Weis, A.; Bein, T. Formation of stable 2D Methylammonium Antimony Iodide Phase for Lead-free Perovskite-like Solar Cells. *J. Phys.: Energy* **2020**, *2*, 024007.
(16) Chatterjee, S.; Pal, A. J. Tin(IV) Substitution in $(CH_3NH_3)_3Sb_2I_9$: Towards Low Band Gap Defect-Ordered Hybrid Perovskite Solar Cells. *ACS Appl. Mater. Interfaces* **2018**, *10*, 35194−35205.
(17) Saparov, B.; Hong, F.; Sun, J. P.; Duan, H.-S.; Meng, W.; Cameron, S.; Hill, I. G.; Yan, Y.; Mitzi, D. B. Thin-Film Preparation and Characterization of $Cs_3Sb_2I_9$: A Lead-Free Layered Perovskite Semiconductor. *Chem. Mater.* **2015**, *27*, 5622−5632.
(18) Umar, F.; Zhang, J.; Jin, Z.; Muhammad, I.; Yang, X.; Deng, H.; Jahangeer, K.; Hu, Q.; Song, H.; Tang, J. Dimensionality Controlling of $Cs_3Sb_2I_9$ for Efficient All-Inorganic Planar Thin Film Solar Cells by HCl-Assisted Solution Method. *Adv. Opt. Mater.* **2019**, *7*, 1801368.
(19) Singh, A.; Boopathi, K. M.; Mohapatra, A.; Chen, Y. F.; Li, G.; Chu, C. W. Photovoltaic Performance of Vapor-Assisted Solution-Processed Layer Polymorph of $Cs_3Sb_2I_9$. *ACS Appl. Mater. Interfaces* **2018**, *10*, 2566−2573.
(20) Chonamada, T. D.; Dey, A. B.; Santra, P. K. Degradation Studies of $Cs_3Sb_2I_9$: A Lead-Free Perovskite. *ACS Appl. Energy Mater.* **2020**, *3*, 47−55.
(21) (a) Johnston, A.; Dinic, F.; Todorovic, P.; Chen, B.; Sagar, L. K.; Saidaminov, M. I.; Hoogland, S.; Voznyy, O.; Sargent, E. H. Narrow Emission from $Rb_3Sb_2I_9$ Nanoparticles. *Adv. Opt. Mater.* **2020**, *8*, 1901606. (b) Li, Y.; Xu, Z.; Liu, X.; Tao.; et al. Two Heteromorphic Crystals of Antimony-Based Hybrids Showing Tunable Optical Band Gaps and Distinct Photoelectric Responses. *Inorg. Chem.* **2019**, *58*, 6544−6549.
(22) (a) Harikesh, P. C.; Mulmudi, H. K.; Ghosh, B.; Goh, T. W.; Teng, Y. T.; Thirumal, K.; Lockrey, M.; Weber, K.; Koh, T. M.; Li, S.; Mhaisalkar, S.; Mathews, N. Rb as an Alternative Cation for Templating Inorganic Lead-Free Perovskites for Solution Processed Photovoltaics. *Chem. Mater.* **2016**, *28*, 7496−7504. (b) Jia, X.; Ding, L. A Low-temperature Solution-processed Copper Antimony Iodide Rudorffite for Solar Cells. *Sci. China Mater.* **2019**, *62*, 54−58.
(23) (a) Weber, S.; Rath, T.; Fellner, K.; Fischer, R.; Resel, R.; Kunert.; et al. Influence of the Iodide to Bromide Ratio on Crystallographic and Optoelectronic Properties of Rubidium Antimony Halide Perovskites. *ACS Appl. Energy Mater.* **2019**, *2*, 539−547. (b) Li, Y.-J.; Wu, T.; Sun, L.; Yang.; et al. Lead-free and Stable Antimony−Silver-Halide Double Perovskite $(CH_3NH_3)_2AgSbI_6$. *RSC Adv.* **2017**, *7*, 35175−35180.
(24) (a) Li, F.; Wang, Y.; Xia, K.; Hoye, R. L. Z.; Pecunia, V. Microstructural and Photoconversion Efficiency Enhancement of Compact Films of Lead-Free Perovskite Derivative $Rb_3Sb_2I_9$. *J. Mater. Chem. A* **2020**, *8*, 4396−4406. (b) Vargas, B.; Ramos, E.; Perez-Gutierrez, E.; Alonso, J. C.; Solis-Ibarra, D. A Direct Bandgap Copper−Antimony Halide Perovskite. *J. Am. Chem. Soc.* **2017**, *139*, 9116−9119.
(25) (a) Nie, R.; Mehta, A.; Park, B.-W.; Kwon, H.-W.; Im, J.; Seok, S. I. Mixed sulfur and iodide-based lead-free perovskite solar cells. *J. Am. Chem. Soc.* **2018**, *140*, 872−875. (b) Nie, R.; Mehta, A.; Park, B.-W.; Kwon, H.-W.; Im, J.; Seok, S. I. Mixed sulfur and iodide-based lead-free perovskite solar cells. *J. Am. Chem. Soc.* **2018**, *140*, 872−875.

https://dx.doi.org/10.1021/acsomega.0c04174
ACS Omega 2020, 5, 28404−28412